Formation Mechanism of β-Li_3PS_4 through Decomposition of Complexes

Marcela Calpa,[a,b] Hiroshi Nakajima,[c] Shigeo Mori,[c] Yosuke Goto,[d] Yoshikazu Mizuguchi,[d] Chikako Moriyoshi,[e] Yoshihiro Kuroiwa,[e] Nataly Carolina Rosero-Navarro,[b] Akira Miura,[b*] Kiyoharu Tadanaga[b]

[a] Graduate School of Chemical Sciences and Engineering, Hokkaido University, Sapporo 060-8628, Japan.

[b] Faculty of Engineering, Hokkaido University, Sapporo 060-8628, Japan.

[c] Department of Materials Science, Osaka Prefecture University, Sakai, Osaka 599-8531, Japan

[d] Department of Physics, Tokyo Metropolitan University, Hachioji 192-0397, Japan.

[e] Graduate School of Advanced Science and Engineering, Hiroshima University, Kagamiyama, Higashihiroshima, 739-8526, Japan

Abstract

β-Li_3PS_4 is a solid electrolyte with high Li^+ conductivity, applicable to sulfide-based all-solid-state batteries. While β-Li_3PS_4 synthesized solid-state reaction forms only in a narrow 300–400 °C temperature range upon heating, β-Li_3PS_4 is readily available by liquid-phase synthesis through low-temperature thermal decomposition of complexes composed of PS_4^{3-} and various organic solvents. However, the conversion mechanism of β-Li_3PS_4 from these complexes has not been yet understood. Herein, we proposed the synthesis mechanism of β-Li_3PS_4 from Li_3PS_4·acetonitrile (Li_3PS_4·ACN) and Li_3PS_4·1,2-dimethoxyethane (Li_3PS_4·DME), whose structural similarity with β-Li_3PS_4 would reduce the nucleation barrier for the formation of β-Li_3PS_4. Synchrotron X-ray diffraction clarified that both the complexes possess similar layered structures consisting of alternating $Li_2PS_4^-$ and Li^+-ACN/DME layers. ACN/DME was removed from these complexes upon heating, and rotation of the PS_4 tetrahedra induced a uniaxial compression to form the β-Li_3PS_4 framework.

Introduction

The synthesis of polymorphs, i.e., different structures with the same composition, attracts great scientific interests,[1-4] and is important for utilizing their excellent properties, such as catalysts,[5-6] solid electrolytes,[7-8] and superconductors[9-10]. The formation energies of different polymorphs often have small differences;[11] therefore, approaches that control the kinetics need to be developed. Rate-limited kinetics of the reactions to form target compounds can be understood as diffusion, nucleation, or crystal growth. However, the required reaction conditions for diffusing all the components, nucleate, and grow a targeted polymorph are often very challenging to find.[12] In particular, the temperature requirements of diffusion and nucleation for producing polymorphs are conflicting. An increase in temperature is favored for enhancing diffusion to complete the reaction; however, it often loses selectivity by exceeding the kinetic barrier of the nucleation of the most stable phase. In contrast, a decrease in temperature favors the kinetic trapping of polymorphs, not by overcoming the nucleation barrier of stable phases; however, reactions may not proceed because of low diffusion rates of components and/or may prevent the nucleation of polymorphs.[13]

The choice of starting materials is another factor that affords the phase selectivity of polymorphs. Single-source precursors, comprising all the elements of the targeted material with organic molecules in one compound, have been widely used in low-temperature approaches to produce polymorphs.[14-16] Low-temperature heating of single-source precursors removes organic molecules, thereby resulting in phase conversion into target materials. Atomically mixed components in a precursor need only short-range diffusion, making nucleation a rate-limiting step. Structural similarity between precursors and target products decreases the nucleation barriers. Successful examples of the synthesis of materials from complexes are brookite-TiO_2,[14] zinc blende-SnS,[15] and cubic GaN[16].

Sulfide-based solid electrolytes are key materials for all-solid-state lithium batteries owing to their high room-temperature ionic conductivity[17-20] and good ductility[20-22]. Li_3PS_4 are typical sulfide electrolytes having three polymorphs, i.e., α-, β-, and γ-Li_3PS_4 with different arrangements of PS_4^{3-}

polyanions.[23] The preparation of sulfide electrolytes generally involves the solid-state reaction of mixed Li_2S and P_2S_5 powders[24-25] or liquid-phase reaction of these powders in organic solvents.[26-28] Through a solid-state reaction, β-Li_3PS_4 is obtained only within a narrow temperature range of 300–400 °C.[23, 29] Heating at a higher temperature produces α-Li_3PS_4 phase and cooling yields γ-Li_3PS_4 phase,[29] attesting to the metastability of β-Li_3PS_4 near room temperature. In comparison, an interesting feature of the liquid-phase synthesis is thatβ-Li_3PS_4 is obtained by the formation of Li_3PS_4 complexes (Li_3PS_4·acetonitrile[30], Li_3PS_4·tetrahydrofuran[8], Li_3PS_4·ethyl propionate[31] and Li_3PS_4·ethyl acetate[32]) in organic solvents and the subsequent thermal decomposition below 250 °C of these complexes.[8, 33] The all-solid-state batteries composed of β-Li_3PS_4 synthesized through the formation of complexes, Li(Ni, Mn, Co)O_2 and Li metal show good cycle performances.[34] However, why and how β-Li_3PS_4 is synthesized from these complexes synthesized in organic solvents is not yet clear. Additionally, the structures of complexes have not been determined except Li_3PS_4·1,2-dimethoxyethane (Li_3PS_4·DME) complex,[35] which is used for the synthesis of Li_4PS_4I solid electrolytes by adding LiI, not β-Li_3PS_4.

Herein, we proposed the formation mechanism by which β-Li_3PS_4 is formed through thermal decomposition of complex precursors. The crystal structure of Li_3PS_4·acetonitrile (Li_3PS_4·ACN) was determined, and the transformation mechanism from Li_3PS_4·ACN to β-Li_3PS_4 through its uniaxial compression is proposed, and possible Li^+ conducting path in β-Li_3PS_4 deduced from the structure of complexes are discussed. The structural similarity of Li_3PS_4·DME and Li_3PS_4·ACN and their parallel decomposition processes identify these materials as useful precursors of β-Li_3PS_4.

1. Experimental

2.1 Synthesis

Li_2S (Mitsuwa Chemical, 99.9%) and P_2S_5 (Aldrich, 99%) were mixed with stoichiometric composition of 3 to 1 in anhydrous acetonitrile (ACN, Wako Pure Chemical Industries 99.5%) or 1,2-

Dimethoxyethane (DME, Sigma Aldrich 99.5%) using magnetic stirring for 2-7 days at 50 °C. Each sample was subsequently dry at 50 °C under vacuum for 2 h to remove excess of solvent.

2.2 Characterization

Synchrotron X-ray powder diffraction (PXRD) measurements were performed at the beamline BL02B2 of SPring-8 with the approval of the Japan Synchrotron Radiation Research Institute (JASRI) (Proposal number 2018B1246). The wavelength was λ= 0.496353(1) Å, and measurement temperature was room temperature. The sample was sealed in a glass capillary with a diameter of 0.2 mm and intensity data were collected using a high-resolution one-dimensional semiconductor detector, multiple MYTHEN system[36]. Initial model was proposed by using EXPO-2014[37], and further refinement was performed by RIETAN-FP[38]. Electron density was derived by a maximum entropy method using Dysnomia[39]. Crystal structure and electron density were drawn by VESTA[40].

The ionic conductivity of the pelletized samples was evaluated by electrochemical impedance spectroscopy (EIS). The solid electrolyte powders (60 mg) were pressed under 360 MPa (at room temperature) in a polycarbonate tube, with a 10 mm diameter; two stainless steel (SS) disks were used as current collectors. EIS was measured using an impedance analyser (SI 1260, Solartron) in the frequency range from 0.1 Hz to 1 MHz at the amplitude of 30 mV. The spectra were analyzed with ZView software (Version 3.3f, Scribner Associates) in order to assess the ohmic resistance (R) of the pellet.

2.3 Computational

DFT calculation was performed using the Vienna ab initio software package (VASP)[41-42], using the projector augmented-wave method with the GGA-PBE functional. The k-point densities were distributed within the Brillouin zone in a Monkhorst–Pack grid[43] of 3×3×2 or 2×2×2. Plane-wave basis cut-off energies are set to 300 eV. The lattice parameters and atomic positions were optimized until the residual force reaches below 0.04 eV/ Å.

3. Results and Discussion

3.1. Crystal structure of Li_3PS_4·ACN

The crystal structure of Li_3PS_4·ACN was successfully proposed based on the synchrotron XRD. The direct method implanted in the EXPO 2014 software[37] produced the initial model with the unit cell of the $P4_2/nbc$ space group with the lattice parameters of a~8.59 and c~12.8 Å together with reasonable atomic positions within the PS_4 tetrahedron and a linear representation of the ACN molecule. Partial occupancies of Li^+ improved the refinement parameters. Final Rietveld analysis to minimize residual electron density assuming the same molar ratio of Li_3PS_4 and ACN converged with reasonable R-factors: R_{wp}=3.02 and R_p=2.29 %. Figure 1(a) shows the corresponding Rietveld profile.

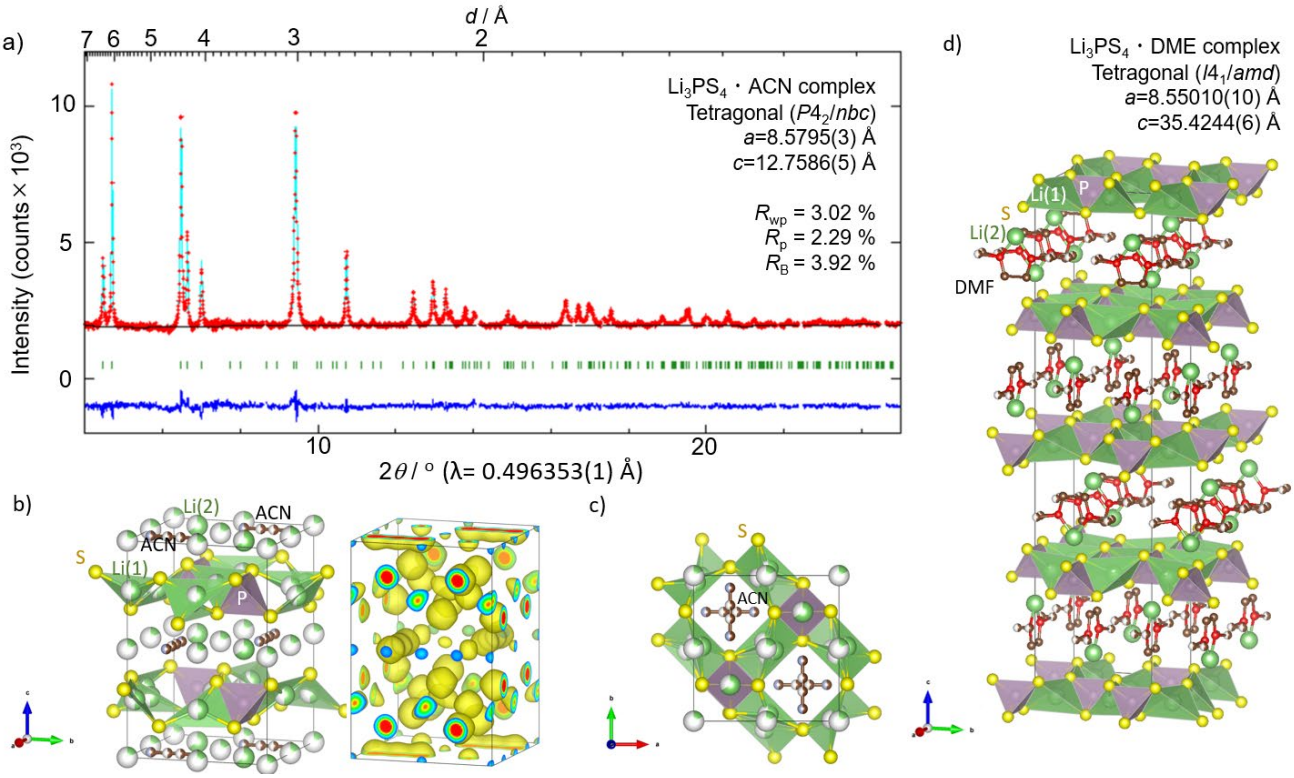

Figure 1. SXRD pattern and proposed crystal structure of Li_3PS_4·ACN compared with that of Li_3PS_4·DME. a) Rietveld refinement of Li_3PS_4·ACN. Diffraction of residual Li_2S is removed. Observed (dot), calculated (line), and difference (bottom line) patterns are shown. Vertical bars denote the positions

of Bragg reflections. b,c) Crystal structure of Li_3PS_4·ACN. The corresponding electron density distribution of Li_3PS_4·ACN is shown at an equi-density level of 0.6 Å. d) Structural model of Li_3PS_4·DME.[35]

Figures 1(b) and 1(c) show the crystal structure of Li_3PS_4·ACN proposed by the Rietveld refinement. The crystal structure is represented as a layered configuration comprising $Li_2PS_4^-$ layers and interposed Li^+ and ACN molecules. Lithium ions in the $Li_2PS_4^-$ layers are arrayed in distorted tetrahedra, and interlayered Li^+ ions are located in a rectangular plane. A statistical distribution of Li^+ improves the fitting parameters. The top view shows the channels containing the ACN molecules.

The P–S distance of 2.026(3) Å in the PS_4 tetrahedron is comparable to that in Li_3PS_4 crystals (~2.03 Å in β-Li_3PS_4[29]). The C_2H_3N molecules are represented by partially occupied symmetric C/N–C–C–C/N bonds without three H. The distance between two C/N units is 2.844(17) Å, which is slightly longer than the linear N≡C–C distance in acetonitrile (2.585(3) Å).[44] This difference is attributed to displacement of the ACN molecules and/or the lack of electron density related to the absence of three H. However, electron densities derived by the maximum entropy method provide a reasonable representation of linear ACN molecules. Li^+ ions occurring in highly occupied sites bind to the negatively charged nitrogen in ACN molecules, which explains the stability of Li_3PS_4·ACN even above the boiling temperature of ACN (355 K).

The crystal structure of Li_3PS_4·ACN is similar to that of Li_3PS_4·DME.[35] Both structures are tetragonal and consist of alternate $Li_2PS_4^-$ layers and interposed Li^+ layers bonded to organic molecules. Both display ABAB stacking of $Li_2PS_4^-$ layers. Whereas the stacking of organic molecules in Li_3PS_4·ACN is ABAB, it is ABCDABCD in Li_3PS_4·DME. Thus, the *a*-axis lattice parameters of both complexes are comparable, but the *c*-axis parameter is larger in the DME derivative. Whereas the Li^+ positions in Li_3PS_4·ACN is proposed to be partially occupied sites, those sites are fully occupied in Li_3PS_4·DME.

Nuetron diffraction study is desired to discuss this difference because X-ray scattering factor of Li^+ is small.

3.2. Conversion from Li_3PS_4·ACN/Li_3PS_4·DME to β-Li_3PS_4

SEM images of Li_3PS_4·ACN and Li_3PS_4·DME, shown in figure 2, exhibit plate crystals, which are typical for materials having layered structures. XRD patterns of Li_3PS_4·ACN and Li_3PS_4·DME are similar to the XRD patterns simulated from the corresponding crystal structures. The formation of Li_3PS_4·ACN was also supported by electron diffraction (Figure S1). The heat treatment of both complexes produces β-Li_3PS_4, in agreement with the reported behavior of Li_3PS_4·ACN.[45] The weight losses of Li_3PS_4·ACN and Li_3PS_4·DME are 18.4 and 33.6%, respectively, which agree with values of 18.6 and 33.4%, respectively, expected from the chemical formulas. Figure 3 shows the temperature dependence of conductivity of the synthesized β-Li_3PS_4. The Li^+ conductivities and activation energies of the synthesized β-Li_3PS_4 are respectively ~0.1 $mS \cdot cm^{-1}$ and~26-30 kJ mol^{-1}, which are comparable to other β-Li_3PS_4 synthesized by the decomposition of complexes.[8, 26-27, 33]

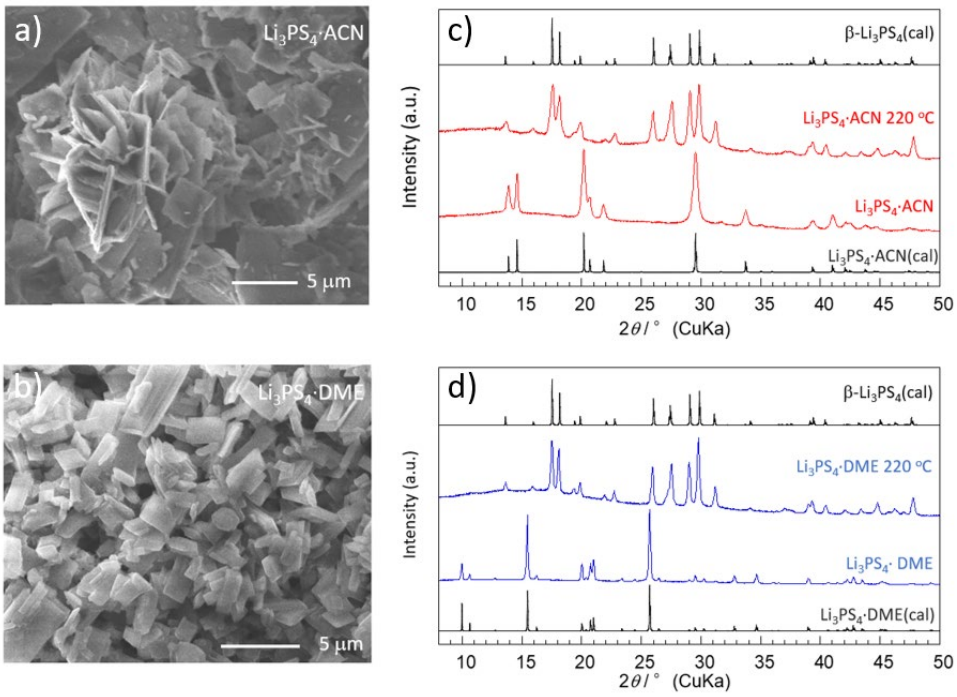

Figure 2. a) and b) SEM images of Li_3PS_4·ACN and Li_3PS_4·DME complexes, respectively. c) and d) XRD patterns before and after heat treatment at 220 °C of Li_3PS_4·ACN and Li_3PS_4·DME, respectively. Simulated patterns from CIF data are shown for comparison.[35]

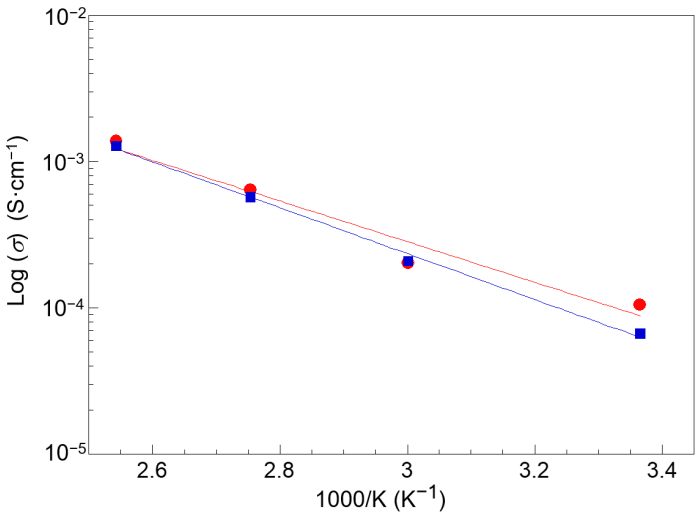

Figure 3. Temperature dependency of the ionic conductivity of β-Li_3PS_4 obtained from Li_3PS_4·ACN (red) and Li_3PS_4·DME (blue). β-Li_3PS_4 from Li_3PS_4·ACN exhibited an ionic conductivity of 1 x 10^{-4} S cm^{-1} at room temperature. and an activation energy of 26.8 kJ mol^{-1}. Li_3PS_4·DME exhibited an ionic conductivity of 0.7 x 10^{-4} S

cm^{-1} at room temperature and an activation energy of 30.5 kJ mol^{-1}. The density of pelletized samples was 1.5 g/cm^3 in both samples.

3.3. Conversion mechanism from Li_3PS_4·ACN/Li_3PS_4·DME to β-Li_3PS_4

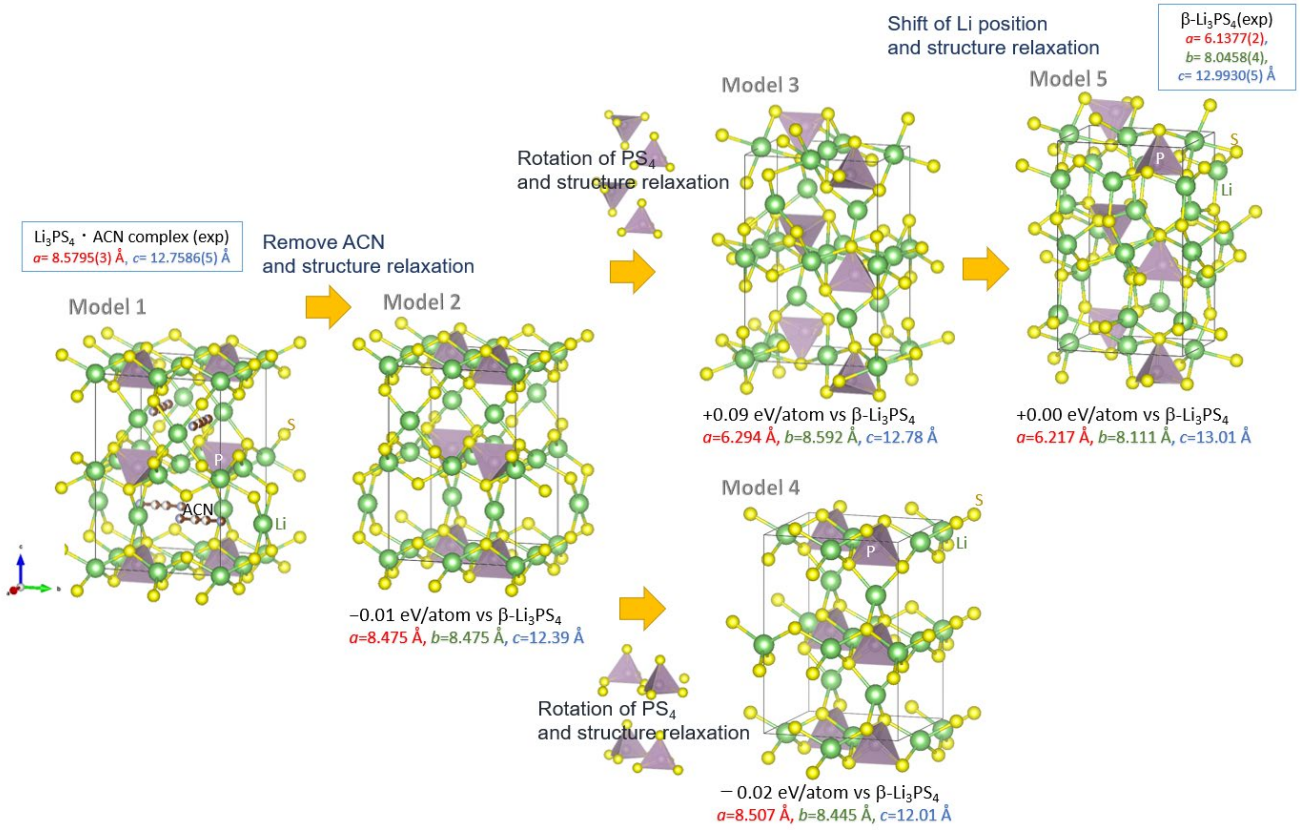

Figure 4. Proposed mechanism of Li_3PS_4·ACN decomposition to β-Li_3PS_4. Minus energy means high thermodynamic stability. To illustrate the structural similarity, the origin of Li_3PS_4·ACN is shifted and the *a*- and *c*-axes of β-Li_3PS_4 are transformed. Structural refinement was performed by DFT calculation in VASP.[41]

The structural similarity between Li_3PS_4·ACN and Li_3PS_4·DME suggests that both materials decompose by a similar mechanism. We used Li_3PS_4·ACN with the smaller unit cell to construct a decomposition model. Figure 4 illustrates the simplified mechanism comprising the uniaxial compression of Li_3PS_4·ACN to β-Li_3PS_4 by removal of ACN, rotation of PS_4 tetrahedra, and a shift of Li^+ ions. After

each step in the process, DFT calculation relaxed the structures by optimizing the lattice parameters and all atomic positions. Li^+ positions are simplified as being fully occupied in each structure by merging partial Li^+ occupancies into an intermediate position between full and half occupancies. Positions with low occupancies are ignored. To illustrate the structural similarity, the origin of the structure is shifted (Model 1), the *a*- and *c*-axes of β-Li_3PS_4 are transformed (Model 5), and the *b*-axis is unchanged.

Structural Model 2 maintains its framework after removal of ACN and subsequent structural optimization. The lattice parameters and atomic coordinates are not significantly changed by structural optimization. The thermodynamic driving force for ACN removal is derived partially from the entropy gain in forming ACN gas. The energies calculated for the structure without ACN nearly equal those of β-Li_3PS_4 (Model 5). Thus, the subsequent steps proceed without a large thermodynamic driving force. Rotation of the PS_4 tetrahedra was visualized in two ways. One model considers the alternate upward and downward orientation of PS_4 apexes to be similar to the PS_4 arrangement in β-Li_3PS_4. The other one considers all PS_4 apexes to be aligned in the same direction as in ɤ-Li_3PS_4. Subsequent DFT calculation of the model comprising alternate upward and downward PS_4 apexes reveals the uniaxial compression along the *a*-axis (see the movie in Supporting Information) that leads to optimized lattice parameters similar to those of β-Li_3PS_4 (Model 3). Thermodynamically, the model 3 is slightly unfavorable over Model 2 and 5. DFT relaxation of the model with all PS_4 apexes aligned in the same direction reverts to a structure similar to that of Model 2 except for a 90° rotation of every other layer (Model 4). This result indicates that the reaction does not proceed. Therefore, rotation of the PS_4 tetrahedra in different directions generates the framework ofβ-Li_3PS_4, which reduces the nucleation barrier to the formation of β-Li_3PS_4. In this way, β-Li_3PS_4, not ɤ-Li_3PS_4, is formed from Li_3PS_4·ACN. Finally, a shift of two-thirds of the Li^+ positions and further optimization results in the formation of β-Li_3PS_4 (Model 5). This reorganization is understandable based on Li^+ ion mobility. The transformation mechanism suggests that the framework of the $Li_2PS_4^-$ layers is decisive in producingβ-Li_3PS_4.

The displacement factors of Li sites in β-Li_3PS_4 is enormously high.[23, 29, 46-47] The positions of Li^+ sites with partial occupancy depend on the synthetic method, measurement temperature, and diffraction technique.[23, 29, 46-47] The lithium-ion conduction path is reported to traverse the network of partially occupied Li sites in the PS_4 units along the [010] and/or [101] direction. Model 3, which contains a high Li concentration along the [010] direction, is slightly unstable relative to β-Li_3PS_4 (Model 5). However, we cannot eliminate the possibility that the Li^+ positions in Model 3 are reasonable, because the models are simplified by ignoring the partial occupancies of Li. Moreover, a variety of structural models with comparable formation energies and different Li positions can stabilize their structures by entropy gain. Thus, Model 3, in which Li^+ transport occurs in the [010] direction, potentially accounts for the high conductivity of β-Li_3PS_4 synthesized from Li_3PS_4·ACN compared with that of β-Li_3PS_4 synthesized by solid-state reaction. Structural models become more complicated when the hydrogen incorporation suggested by Kaup et al.[23] and the dynamical movement of constituent atoms are considered.[48] Further investigation of the effect of highly mobile Li^+ and H^+ on the decomposition mechanism is needed because various Li^+ configurations and H^+ incorporation impact the stability and conductivity of β-Li_3PS_4.

4. Conclusion

We propose the formation mechanism of metastable β-Li_3PS_4 from Li_3PS_4·ACN and Li_3PS_4·DME. Both the complex, which contain alternating $Li_2PS_4^-$ and Li^+-ACN/DME layers, yield metastable β-Li_3PS_4 upon heating at 220 °C in an inert atmosphere. The transformation mechanism is viewed as a uniaxial compression combined with the rotation of PS_4 tetrahedra in different directions, which reduces the nucleation barrier for metastable β-Li_3PS_4 formation. Considering various polymorph structures are derived during the proposed decomposition of complexes, this work will help to understand the conduction path in metastable electrolytes from the structure of complex precursors, pushing rational design of highly conducting electrolytes with superior conducting path in the future.

SUPPORTING DOCUMENTS

TEM images, structural analysis detail, CIF file for $Li_3PS_4 \cdot ACN$, and the movie of DFT optimization.

Conflicts of interest

There are no conflicts to declare.

ACKNOWLEDGMENT

AM acknowledges Profs. K. Hirai, Y. Kitagawa and Y. Hasegawa (Hokkaido Univ.) for the suggestions about complexes, Prof. D. Urushihara (Nagoya Institute of Technology) for the advice for structural refinement. AM, GY, and YM thank Dr. S. Kawaguchi (JASRI) for technical support for synchrotron measurement in SPring-8 with the approvals of 2018B1246. This research was partially supported by KAKENHI Grant Numbers JP19H04682, JP20KK0124, JP21H01610.

REFERENCES

1. Leonard, B. M.; Bhuvanesh, N. S. P.; Schaak, R. E., Low-Temperature Polyol Synthesis of $AuCuSn_2$ and $AuNiSn_2$: Using Solution Chemistry to Access Ternary Intermetallic Compounds as Nanocrystals. *J. Am. Chem. Soc.* **2005,** *127* (20), 7326-7327.
2. Amano, S.; Bogdanovski, D.; Yamane, H.; Terauchi, M.; Dronskowski, R., varepsilon-TiO, a Novel Stable Polymorph of Titanium Monoxide. *Angew. Chem. Int. Ed. Engl.* **2016,** *55* (5), 1652-7.
3. Todd, P. K.; Neilson, J. R., Selective formation of yttrium manganese oxides through kinetically competent assisted metathesis reactions. *J. Am. Chem. Soc.* **2019,** *141* (3), 1191-1195.
4. Fischer, D.; Jansen, M., Synthesis and Structure of Na3N. *Angew. Chem. Int. Ed.* **2002,** *41* (10), 1755-1756.
5. Lin, H.; Li, L.; Zhao, M.; Huang, X.; Chen, X.; Li, G.; Yu, R., Synthesis of high-quality brookite TiO_2 single-crystalline nanosheets with specific facets exposed: tuning catalysts from inert to highly reactive. *J. Am. Chem. Soc.* **2012,** *134* (20), 8328-31.
6. Robinson, D. M.; Go, Y. B.; Mui, M.; Gardner, G.; Zhang, Z.; Mastrogiovanni, D.; Garfunkel, E.; Li, J.; Greenblatt, M.; Dismukes, G. C., Photochemical water oxidation by crystalline polymorphs of manganese oxides: structural requirements for catalysis. *J. Am. Chem. Soc.* **2013,** *135* (9), 3494-501.
7. Tatsumisago, M.; Shinkuma, Y.; Minami, T., Stabilization of superionic α-AgI at room temperature in a glass matrix. *Nature* **1991,** *354* (6350), 217-218.
8. Liu, Z. C.; Fu, W. J.; Payzant, E. A.; Yu, X.; Wu, Z. L.; Dudney, N. J.; Kiggans, J.; Hong, K. L.; Rondinone, A. J.; Liang, C. D., Anomalous High Ionic Conductivity of Nanoporous β-Li_3PS_4. *J. Am. Chem. Soc.* **2013,** *135* (3), 975-978.
9. Martinolich, A. J.; Kurzman, J. A.; Neilson, J. R., Polymorph selectivity of superconducting $CuSe_2$ through kinetic control of solid-state metathesis. *J. Am. Chem. Soc.* **2015,** *137* (11), 3827-33.
10. Nagao, M.; Miura, A.; Urushihara, D.; Maruyama, Y.; Goto, Y.; Mizuguchi, Y.; Moriyoshi, C.; Kuroiwa, Y.; Wang, Y.; Watauchi, S.; Asaka, T.; Takano, Y.; Tadanaga, K.; Tanaka, I., Flux Growth and Superconducting Properties of (Ce,Pr)$OBiS_2$ Single Crystals. *Front Chem* **2020,** *8*, 44.
11. Sun, W.; Dacek, S. T.; Ong, S. P.; Hautier, G.; Jain, A.; Richards, W. D.; Gamst, A. C.; Persson, K. A.; Ceder, G., The thermodynamic scale of inorganic crystalline metastability. *Sci. Adv.* **2016,** *2* (11), e1600225-e1600225.
12. Cordova, D. L. M.; Johnson, D. C., Synthesis of Metastable Inorganic Solids with Extended Structures. *ChemPhysChem* **2020,** *21* (13), 1345-1368.
13. Stein, A.; Keller, S. W.; Mallouk, T. E., Turning Down the Heat: Design and Mechanism in Solid-State Synthesis. *Science* **1993,** *259* (5101), 1558.

14. Tomita, K.; Petrykin, V.; Kobayashi, M.; Shiro, M.; Yoshimura, M.; Kakihana, M., A Water-Soluble Titanium Complex for the Selective Synthesis of Nanocrystalline Brookite, Rutile, and Anatase by a Hydrothermal Method. *Angew. Chem. Int. Ed.* **2006,** *45* (15), 2378-2381.
15. Ahmet, I. Y.; Hill, M. S.; Johnson, A. L.; Peter, L. M., Polymorph-Selective Deposition of High Purity SnS Thin Films from a Single Source Precursor. *Chem. Mater.* **2015,** *27* (22), 7680-7688.
16. Sardar, K.; Dan, M.; Schwenzer, B.; Rao, C. N. R., A simple single-source precursor route to the nanostructures of AlN, GaN and InN. *J. Mater. Chem.* **2005,** *15* (22), 2175-2177.
17. Hayashi, A.; Sakuda, A.; Tatsumisago, M., Development of Sulfide Solid Electrolytes and Interface Formation Processes for Bulk-Type All-Solid-State Li and Na Batteries. *Frontiers in Energy Research* **2016,** *4*.
18. Kato, Y.; Hori, S.; Saito, T.; Suzuki, K.; Hirayama, M.; Mitsui, A.; Yonemura, M.; Iba, H.; Kanno, R., High-power all-solid-state batteries using sulfide superionic conductors. *Nat. Energy* **2016,** *1*, 7.
19. Zheng, F.; Kotobuki, M.; Song, S.; Lai, M. O.; Lu, L., Review on solid electrolytes for all-solid-state lithium-ion batteries. *J. Power Sources* **2018,** *389*, 198-213.
20. Chen, S.; Xie, D.; Liu, G.; Mwizerwa, J. P.; Zhang, Q.; Zhao, Y.; Xu, X.; Yao, X., Sulfide solid electrolytes for all-solid-state lithium batteries: Structure, conductivity, stability and application. *Energy Storage Materials* **2018,** *14*, 58-74.
21. Kudu, Ö. U.; Famprikis, T.; Fleutot, B.; Braida, M.-D.; Le Mercier, T.; Islam, M. S.; Masquelier, C., A review of structural properties and synthesis methods of solid electrolyte materials in the Li2S− P2S5 binary system. *J. Power Sources* **2018,** *407*, 31-43.
22. Sakuda, A.; Hayashi, A.; Tatsumisago, M., Sulfide Solid Electrolyte with Favorable Mechanical Property for All-Solid-State Lithium Battery. *Sci Rep* **2013,** *3*, 1-5.
23. Kaup, K.; Zhou, L.; Huq, A.; Nazar, L. F., Impact of the Li substructure on the diffusion pathways in alpha and beta Li_3PS_4: an in situ high temperature neutron diffraction study. *J. Mater. Chem. A* **2020**.
24. Hayashi, A.; Hama, S.; Morimoto, H.; Tatsumisago, M.; Minami, T., Preparation of $Li_2S–P_2S_5$ Amorphous Solid Electrolytes by Mechanical Milling. *J. Am. Ceram. Soc.* **2001,** *84* (2), 477-79.
25. Mizuno, F.; Hayashi, A.; Tadanaga, K.; Tatsumisago, M., New, Highly Ion-Conductive Crystals Precipitated from $Li_2S–P_2S_5$ Glasses. *Adv. Mater.* **2005,** *17* (7), 918-921.
26. Miura, A.; Rosero-Navarro, N. C.; Sakuda, A.; Tadanaga, K.; Phuc, N. H.; Matsuda, A.; Machida, N.; Hayashi, A.; Tatsumisago, M., Liquid-phase syntheses of sulfide electrolytes for all-solid-state lithium battery. *Nature Reviews Chemistry* **2019,** *3* (3), 189-198.
27. Ghidiu, M.; Ruhl, J.; Culver, S. P.; Zeier, W. G., Solution-based synthesis of lithium thiophosphate superionic conductors for solid-state batteries: a chemistry perspective. *J. Mater. Chem. A* **2019,** *7* (30), 17735-17753.
28. Yamamoto, K.; Yang, S.; Takahashi, M.; Ohara, K.; Uchiyama, T.; Watanabe, T.; Sakuda, A.; Hayashi, A.; Tatsumisago, M.; Muto, H.; Matsuda, A.; Uchimoto, Y., High Ionic Conductivity of Liquid-Phase-Synthesized Li_3PS_4 Solid Electrolyte, Comparable to That Obtained via Ball Milling. *ACS Applied Energy Materials* **2021,** *4* (3), 2275-2281.
29. Homma, K.; Yonemura, M.; Kobayashi, T.; Nagao, M.; Hirayama, M.; Kanno, R., Crystal structure and phase transitions of the lithium ionic conductor Li_3PS_4. *Solid State Ionics* **2011,** *182* (1), 53-58.
30. Wang, H.; Hood, Z. D.; Xia, Y.; Liang, C., Fabrication of ultrathin solid electrolyte membranes of β-Li 3 PS 4 nanoflakes by evaporation-induced self-assembly for all-solid-state batteries. *J. Mater. Chem. A* **2016,** *4* (21), 8091-8096.
31. Phuc, N. H. H.; Morikawa, K.; Mitsuhiro, T.; Muto, H.; Matsuda, A., Synthesis of plate-like Li_3PS_4 solid electrolyte via liquid-phase shaking for all-solid-state lithium batteries. *Ionics* **2017**, 1-7.
32. Phuc, N. H. H.; Totani, M.; Morikawa, K.; Muto, H.; Matsuda, A., Preparation of Li_3PS_4 solid electrolyte using ethyl acetate as synthetic medium. *Solid State Ionics* **2016,** *288*, 240-243.
33. Wang, H.; Hood, Z. D.; Xia, Y. N.; Liang, C. D., Fabrication of ultrathin solid electrolyte membranes of β-Li_3PS_4 nanoflakes by evaporation-induced self-assembly for all-solid-state batteries. *J. Mater. Chem. A* **2016,** *4* (21), 8091-8096.
34. Randau, S.; Weber, D. A.; Kötz, O.; Koerver, R.; Braun, P.; Weber, A.; Ivers-Tiffée, E.; Adermann, T.; Kulisch, J.; Zeier, W. G.; Richter, F. H.; Janek, J., Benchmarking the performance of all-solid-state lithium batteries. *Nature Energy* **2020,** *5* (3), 259-270.
35. Sedlmaier, S. J.; Indris, S.; Dietrich, C.; Yavuz, M.; Dräger, C.; von Seggern, F.; Sommer, H.; Janek, J., Li_4PS_4I: A Li^+ Superionic Conductor Synthesized by a Solvent-Based Soft Chemistry Approach. *Chem. Mater.* **2017,** *29* (4), 1830-1835.
36. Kawaguchi, S.; Takemoto, M.; Osaka, K.; Nishibori, E.; Moriyoshi, C.; Kubota, Y.; Kuroiwa, Y.; Sugimoto, K., High-throughput powder diffraction measurement system consisting of multiple MYTHEN detectors at beamline BL02B2 of SPring-8. *Rev. Sci. Instrum.* **2017,** *88* (8), 085111.
37. Altomare, A.; Cuocci, C.; Giacovazzo, C.; Moliterni, A.; Rizzi, R.; Corriero, N.; Falcicchio, A., EXPO2013: a kit of tools for phasing crystal structures from powder data. *J. Appl. Crystallogr.* **2013,** *46* (4), 1231-1235.
38. Izumi, F.; Momma, K., Three-dimensional visualization in powder diffraction. *Solid State Phenom.* **2007,** *130*, 15-20.
39. Momma, K.; Ikeda, T.; Belik, A. A.; Izumi, F., Dysnomia, a computer program for maximum-entropy method (MEM) analysis and its performance in the MEM-based pattern fitting. *Powder Diffr.* **2013,** *28* (3), 184-193.
40. Momma, K.; Izumi, F., VESTA: a three-dimensional visualization system for electronic and structural analysis. *J. Appl. Crystallogr.* **2008,** *41* (3), 653-658.
41. Kresse, G.; Furthmüller, J., Efficient iterative schemes for ab initio total-energy calculations using a plane-wave basis set. *Phys. Rev. B* **1996,** *54* (16), 11169-11186.
42. Kresse, G.; Furthmüller, J., Efficiency of ab-initio total energy calculations for metals and semiconductors using a plane-wave basis set. *Computational Materials Science* **1996,** *6* (1), 15-50.
43. Monkhorst, H. J.; Pack, J. D., Special points for Brillouin-zone integrations. *Phys. Rev. B* **1976,** *13* (12), 5188-5192.
44. Brackemeyer, T.; Erker, G.; Fröhlich, R.; Prigge, J.; Peuchert, U., $Cp_3Zr(acetonitrile)^+$: Structure of an Electron-Rich Organometallic d^0-Cation. *Chem. Ber.* **1997,** *130* (7), 899-902.
45. Calpa, M.; Rosero-Navarro, N. C.; Miura, A.; Tadanaga, K., Instantaneous preparation of high lithium-ion conducting sulfide solid electrolyte $Li_7P_3S_{11}$ by a liquid phase process. *RSC Advance* **2017,** *7* (73), 46499-46504.
46. Chen, Y.; Cai, L.; Liu, Z.; dela Cruz, C. R.; Liang, C.; An, K., Correlation of anisotropy and directional conduction in β-Li_3PS_4 fast Li+ conductor. *Appl. Phys. Lett.* **2015,** *107* (1), 013904.
47. Stöffler, H.; Zinkevich, T.; Yavuz, M.; Senyshyn, A.; Kulisch, J.; Hartmann, P.; Adermann, T.; Randau, S.; Richter, F. H.; Janek, J.; Indris, S.; Ehrenberg, H., Li^+-Ion Dynamics in β-Li_3PS_4 Observed by NMR: Local Hopping and Long-Range Transport. *The Journal of Physical Chemistry C* **2018,** *122* (28), 15954-15965.
48. Zhang, Z.; Li, H.; Kaup, K.; Zhou, L.; Roy, P.-N.; Nazar, L. F., Targeting Superionic Conductivity by Turning on Anion Rotation at Room Temperature in Fast Ion Conductors. *Matter* **2020,** *2* (6), 1667-1684.

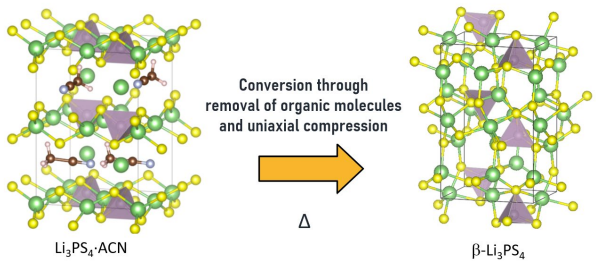

Lithium-ion conductive β-Li_3PS_4 was formed throuth the decomposition of Li_3PS_4·acetonitrile complex accompanied with a uniaxial compression and a rotation of PS_4 units.